applied sciences

MDPI

Article

Research on the Internal Thermal Boundary Conditions of Concrete Closed Girder Cross-Sections under Historically Extreme Temperature Conditions

Jianhui Lin, Junqing Xue *, Fuyun Huang and Baochun Chen

College of Civil Engineering, Fuzhou University, Fuzhou 350108, China; jianhui.lin@foxmail.com (J.L.); huangfuyun@fzu.edu.cn (F.H.); baochunchen@fzu.edu.cn (B.C.)

* Correspondence: junqing.xue@fzu.edu.cn; Tel.: +86-138-5015-2456

Received: 29 November 2019; Accepted: 10 February 2020; Published: 14 February 2020

Featured Application: The temperature distributions on concrete closed girder cross-sections can be accurately simulated by using the finite element models to establish air elements as the internal thermal boundary condition. Using the finite element models to establish air elements as the internal thermal boundary condition has a wide application range because it does not require the field measurement of the temperature inside the cavity, which is cost- and time-prohibitive. Moreover, this method can predict the temperature distributions on concrete closed girder cross-sections under historically extreme temperature conditions.

Abstract: The accuracy of the finite element model (FEM) for concrete closed girder cross-sections is significantly influenced by thermal boundary conditions. The internal thermal boundary conditions can be simulated by inputting the convection heat transfer coefficient and the temperatures inside the cavities or by establishing air elements in the FEM. In order to analyze the influence of different simulation methods for the internal thermal boundary conditions on temperature distributions for concrete closed girder cross-sections, the temperature distributions on the cross-sections of a box girder, small box girders, and adjacent box girders were monitored, and the corresponding FEMs were implemented. By comparing the temperature data obtained from the field test and FEMs, the numerical hourly temperature curves calculated by using the measured temperatures inside the cavities provide the closest agreement with the measured results; however, the measurements of the temperatures on site are cost- and time-prohibitive. When there is a lack of measured temperatures inside the cavities, the numerical hourly temperature curves calculated by establishing air elements in the FEM provide the closest agreement. The influences of different simulation methods for the internal thermal boundary conditions on the highest hourly average effective temperatures and the trends of the vertical temperature gradients for concrete closed girder cross-sections were small. The FEM with air elements can be adopted to analyze the temperature distributions on concrete closed girder cross-sections under historically extreme temperature conditions. It can be predicted that the longitudinal thermal movement of concrete closed girders would be underestimated by considering variations in the one-year measured average effective temperature of the cross-sections or the Chinese-code-specified design effective temperature for the highway bridge structures, which are thus unconservative for engineering applications. The Chinese-code-specified design vertical temperature gradients are conservative for the bridge deck surface and unconservative for the bottom flange.

Keywords: internal thermal boundary condition; concrete closed girder cross-section; air element; finite element simulation; hourly temperature curve; average effective temperature; vertical temperature gradient; historically extreme temperature condition

1. Introduction

Closed girder cross-sections, such as box girders, small box girders, and adjacent box girders, are typically used worldwide for concrete bridges [1–13]. Numerous cases of recorded bridge damages, such as severe cracking, deterioration, or even failure, particularly in bridges with closed girder cross-sections, were caused by temperature-induced stresses and deformations [14–26]. Therefore, it is particularly important to accurately predict the temperature distributions on closed girder cross-sections. Moreover, thermal influence is considered to be a key parameter not only for bridges with expansion joints but also for jointless bridges [7,13,22,27–39]. Finite element simulation is one of the most commonly used and effective methods to analyze the temperature distributions on concrete bridge cross-sections. The accurate input of external and internal thermal boundary conditions for the closed girder cross-sections in the finite element model (FEM) has a great influence on the accuracy of the calculated results. The Robin boundary condition can be used to simulate the external and internal thermal boundary conditions. For the external thermal boundary condition, the temperatures associated with solar radiation, convection, irradiation, and the temperature of the surrounding fluid medium, as well as the overall heat transfer coefficient (which is the combination of the convection heat transfer coefficient and the radiation heat transfer coefficient), should be taken into account [7,13–17,22,23,25,36,39–46]. The internal thermal boundary condition is affected by the temperatures inside the cavities and the convection heat transfer coefficient because it is not influenced by solar radiation [7,13–17,22,23,25,36,39,40,42–46].

The ambient air temperature can be measured by a meteorological station. The temperature variation inside the cavity is usually less than that of the ambient air temperature and has a time delay [42,43] because there is no solar radiation inside the cavity and the thermal conductivity of concrete is low. In order to accurately simulate the internal thermal boundary conditions for concrete closed girder cross-sections, researchers have proposed different methods. Temperature sensors were installed inside the cavities by some researchers during the girder construction process to measure the temperature variation curve inside the cavity (hereafter referred to as the Measured Temperature Method) [17,23,25,39,44]. The Measured Temperature Method can reflect the actual temperature inside the cavity, but measurements on site are cost- and time-prohibitive. Therefore, the application range of the Measured Temperature Method is limited. When the measured temperature inside the cavity can not be obtained, the ambient air temperature was used to simulate the temperature inside the cavity (hereafter referred to as the Ambient Temperature Method) [15,45]. Numerical methods were used by some researchers to calculate the temperature variation curve inside the cavity, such as the mean temperature over the previous two days (hereafter referred to as the Mean Temperature Method) [27,28,41], using the following Equation [40]:

$$T_{\text{mean}} = 0.25 \times (T_{\text{max,i}} + T_{\text{min,i}} + T_{\text{max,i}-1} + T_{\text{min,i}-1}) \quad (1)$$

where T_{mean} is the mean temperature over the previous two days, $T_{\text{max,i}}$, $T_{\text{min,i}}$, $T_{\text{max,i}-1}$, and $T_{\text{min,i}-1}$ are the maximum and minimum temperatures of the ambient air temperature curves for the ith and (i_1)th days.

The temperature inside the cavity that is obtained or calculated by using the Measured Temperature Method, Ambient Temperature Method, or Mean Temperature Method can be input as the internal thermal boundary condition in the FEM. In addition, a method that established air elements in the FEM of the closed girder cross-sections was adopted by some researchers to simulate the heat conduction inside the cavity as the internal thermal boundary condition (hereafter referred to as the Air Element Method) [7,13,25,36,39]. When there is no measurement on site to obtain the temperature inside the cavity, the Ambient Temperature Method, Mean Temperature Method, or Air Element Method can be used as alternative methods. These alternative methods can be used for all bridges; however, their accuracy should be evaluated.

The temperature effects on structures vary with time during the service periods of structures. In order to ensure the safety and durability of bridges, it is necessary to analyze the temperature distributions on concrete girder cross-sections under historically extreme temperature conditions. The Measured Temperature Method, Ambient Temperature Method, and Mean Temperature Method can only be used to simulate the temperature inside the cavity in a specific period based on the measured data. Therefore, it is difficult for them to predict the temperature distributions on concrete girder cross-sections under historically extreme temperature conditions. However, the Air Element Method is expected to be used to simulate the temperature distributions on concrete girder cross-sections under historically extreme temperature conditions.

In this paper, three bridges with different kinds of concrete closed girder cross-sections, including a box girder, small box girders, and adjacent box girders, were chosen as case studies. The temperature distributions on three kinds of concrete closed girder cross-sections were monitored. The corresponding FEMs of the concrete closed girder cross-sections were implemented by using the midas FEA software. Four methods were used to simulate the internal thermal boundary conditions for the concrete closed girder cross-sections. The influences of different simulation methods on the temperature distributions on concrete closed girder cross-sections were analyzed. The Air Element Method was adopted to analyze the temperature distributions on concrete closed girder cross-sections under historically extreme temperature conditions.

2. Finite Element Simulation

2.1. Box Girder

One concrete bridge with a three-cell single box girder in Shenzhen, China was chosen as the case study. The dimensions of the box girder cross-section are illustrated in Figure 1. Twenty-one temperature sensors were installed in the box girder during the construction process, as shown in Figure 1. These include five sensors in the top flange (T-1 to T-5), three sensors in the bottom flange (B-1 to B-3), eight sensors in the exterior webs (W-1 to W-4 in the left exterior web and W-7 to W-10 in the right exterior web), two sensors in the interior webs (W-5 in the left interior web and W-6 in the right interior web), and three sensors (C-1 to C-3) in three cells of the box girder. It can be observed from the field test data that the differences between the temperatures inside the cavities and the ambient air temperature were large in the summer because of high solar radiation, while the temperature differences were small in the winter. The daily measured temperature responses obtained at different times of year have been used by researchers to analyze the temperature distributions on cross-sections [13,22,24,25,39]. Due to space limitations, the data from 13 August 2017 in summer, which is a sunny day with the highest ambient air temperature during the monitoring period, as well as high solar radiation and low wind speed, were selected for analysis. The meteorological data, including ambient air temperature, hourly global solar radiation, hourly diffuse solar radiation, and wind speed, were measured using a movable automatic meteorological station at the bridge site with a measurement time interval of one hour.

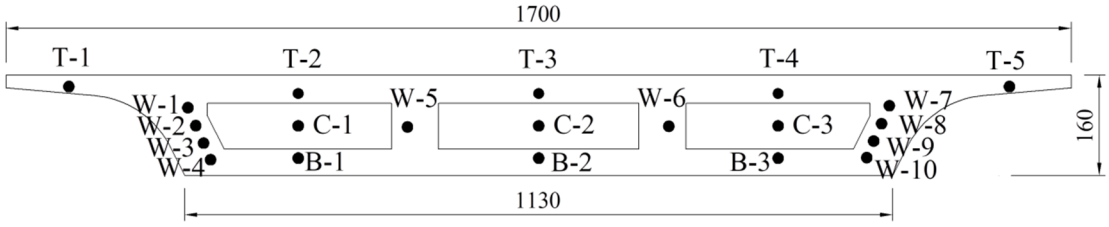

Figure 1. Layout of the box girder cross-section (unit: cm).

The midas FEA software was chosen to establish the FEM for the box girder cross-section. Two-dimensional plane strain elements, which can be used for steady-state or transient analyses,

were used, as shown in Figure 2. Each node has a single temperature degree of freedom. The measurement time interval in the FEM was set with the same as that for the field test. For the thermal parameters of the concrete, density, heat conductivity, and specific heat values of 2500 kg/m^3, 1.5 W/(m·°C), and 900 J/(kg·°C), respectively, were used [14,15,17,47]. Based on the measured ambient air temperature, wind speed, and solar radiation obtained from the movable automatic meteorological station at the bridge site, the parameters associated with solar radiation, convection, irradiation, and the temperature of the surrounding fluid medium were used as the external thermal boundary conditions for the box girder in the FEM. The influence of solar radiation on different parts of the box girder was considered by using the following rules and assumptions: (a) the external surface of the top flange is influenced by both the beam and diffuse solar radiation; (b) the external surfaces of the two exterior webs in the shadow due to the top flange are influenced by the diffuse solar radiation and ground reflection; (c) the external surfaces of the two exterior webs not in the shadow are influenced by the beam solar radiation, diffuse solar radiation, and ground reflection; and (d) the undersides of the top and bottom flanges are influenced by the ground reflection alone. The environmental and climatic conditions existing on previous days must be considered to accurately determine the initial temperature distribution [13,14,17,25,39]. A 120-h period with the same environmental conditions imposed cyclically was considered in the analysis.

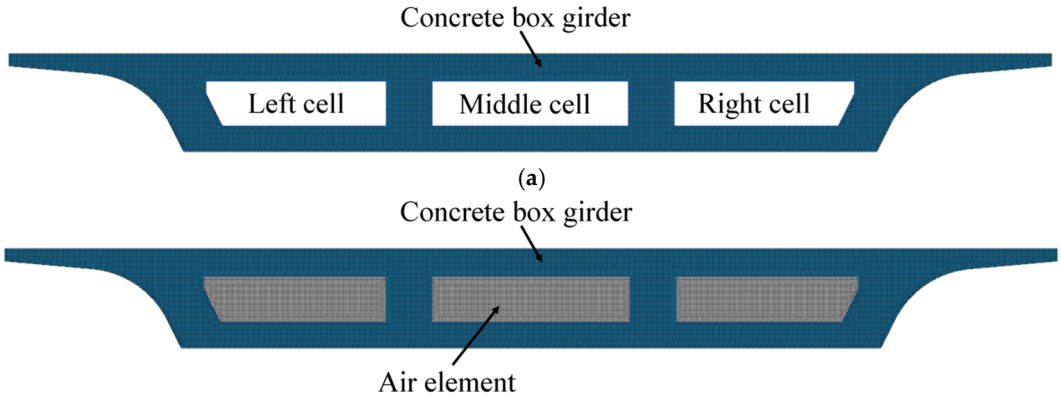

Figure 2. Finite element model (FEM) of the box girder cross-sections: (**a**) FEM without air elements; (**b**) FEM with air elements.

The four simulation methods for the internal thermal boundary conditions summarized in Section 1 were considered in the FEMs of the box girder. The internal thermal boundary condition was not influenced by solar radiation. Therefore, the internal thermal boundary condition with a convection heat transfer coefficient of 3.5 W/(m^2·°C) was set in the FEMs by using the Measured Temperature Method, Ambient Temperature Method, or Mean Temperature Method. For the Measured Temperature Method, the measured hourly temperature curves inside each cell of the box girder (13 August 2017) obtained from the temperature sensors C-1 to C-3 were chosen, as shown by the hollow points in Figure 3. For the Ambient Temperature Method, the measured hourly ambient air temperature curve (13 August 2017) was used, as shown by the solid line in Figure 3. For the Mean Temperature Method, the mean temperature (30.7 °C) over the previous two days (12 and 13 August 2017) was calculated, as shown by the dashed line in Figure 3. The mesh size of the FEMs using the Measured Temperature Method, Ambient Temperature Method, or Mean Temperature Method was set as 20 mm. The total numbers of nodes and elements were 37,017 and 35,659, respectively, as illustrated in Figure 2a. For the Air Element Method, the heat conduction between the air and girder cross-section can be simulated by establishing the air elements inside the cavities without the input of the temperature curves and the convection heat transfer coefficient inside the cavities. The air elements were also

two-dimensional plane strain elements with the thermal parameters of air under 20 °C and one standard atmospheric pressure (density, heat conductivity, and specific heat of 1.205 kg/m^3, 0.0259 W/(m·°C), and 1005 J/(kg·°C), respectively) [48]. The mesh size of the air element was set as 20 mm, which is the same as those of the girder cross-section. The total numbers of nodes and elements for the FEM using the Air Element Method were 52,458 and 51,669, respectively, as illustrated in Figure 2b.

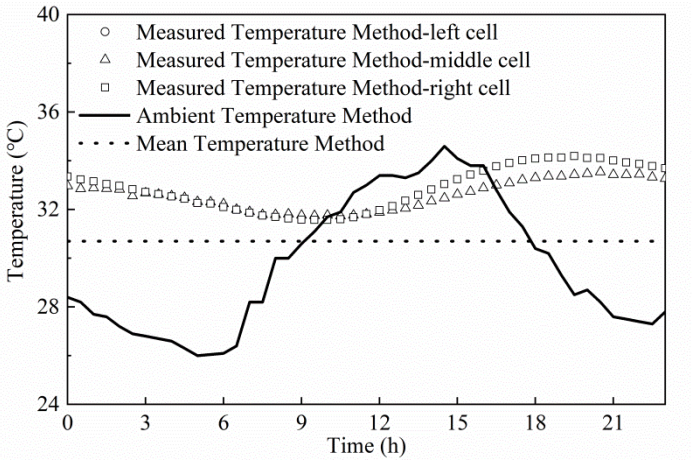

Figure 3. Comparison of different simulation methods for the temperature curves inside the cavities.

2.2. Small Box Girder

One prestressed concrete bridge with a cross-section consisting of seven small box girders in Handan, China was chosen as the case study. A Portland cement concrete overlay with a thickness of 12 cm and an asphalt concrete overlay with a thickness of 10 cm were used. The dimensions of the small box girder cross-sections are illustrated in Figure 4. Six temperature sensors were installed in the top flanges (1-T and 7-T), webs (1-W and 7-W), and bottom flanges (1-B and 7-B) of the small box girders #1 and #7, as shown in Figure 4. Due to space limitations, the data from 17 July 2015 in summer, which is a sunny day with the highest ambient air temperature during the monitoring period, as well as high solar radiation and low wind speed, were selected for analysis. The field test was carried out after bridge opening. Therefore, there was no temperature gauge placed inside the cells of the small box girders. The Measured Temperature Method was not considered in the analyses of the temperature distributions on concrete small box girder cross-sections. The meteorological data, including ambient air temperature, hourly global solar radiation, hourly diffuse solar radiation, and wind speed, were measured using a movable automatic meteorological station at the bridge site with a measurement time interval of one hour.

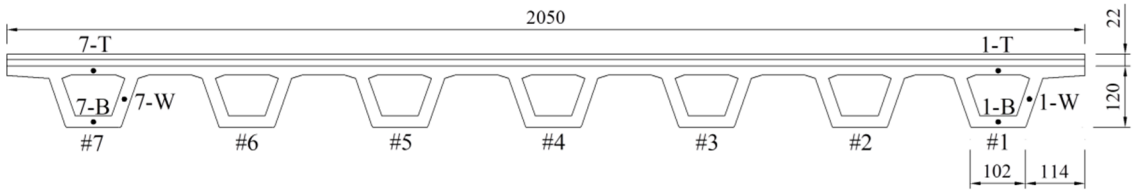

Figure 4. Layout of the small box girder cross-sections (unit: cm).

The midas FEA software was chosen to establish a FEM of the small box girder cross-sections by using two-dimensional plane strain elements, as shown in Figure 5. The three simulation methods for the internal thermal boundary conditions summarized in Section 1, except the Measured Temperature Method, were considered in the FEMs of small box girders. For the Ambient Temperature Method, the measured hourly ambient air temperature curve (17 July 2015) was used, as shown by the solid line in Figure 6. For the Mean Temperature Method, the mean temperature (27.1 °C) over the previous

two days (16 and 17 July 2015) was calculated, as shown by the dashed line in Figure 6. The mesh size of the FEMs using the Ambient Temperature Method or Mean Temperature Method was set as 20 mm. The total numbers of nodes and elements were 34,020 and 32,462, respectively, as illustrated in Figure 5a. For the Air Element Method, the total numbers of nodes and elements for the FEM were 45,632 and 44,786, respectively, as illustrated in Figure 5b. Other detailed information was the same as the FEM of the box girder, as reported in Section 2.1.

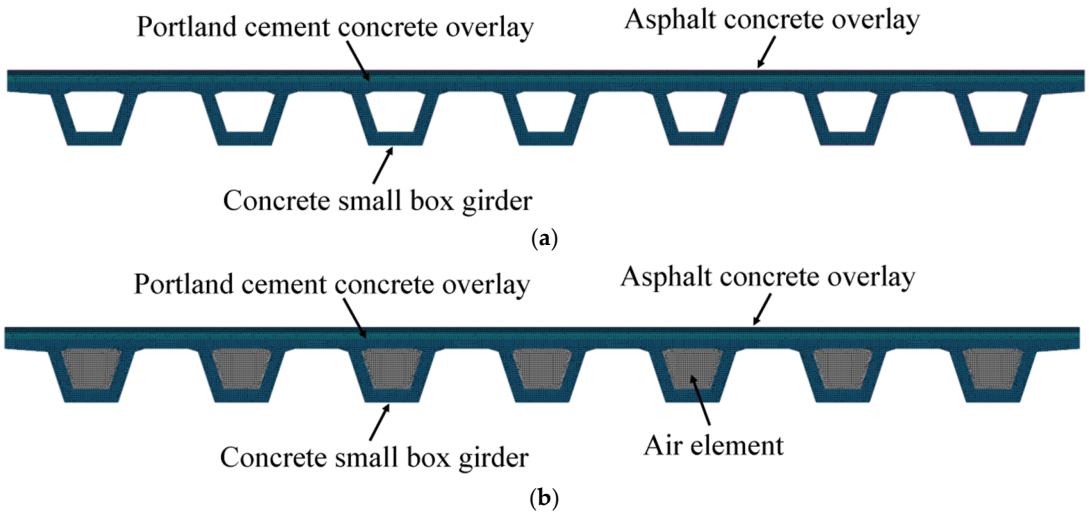

Figure 5. FEM of the small box girder cross-sections: (**a**) FEM without air elements; (**b**) FEM with air elements.

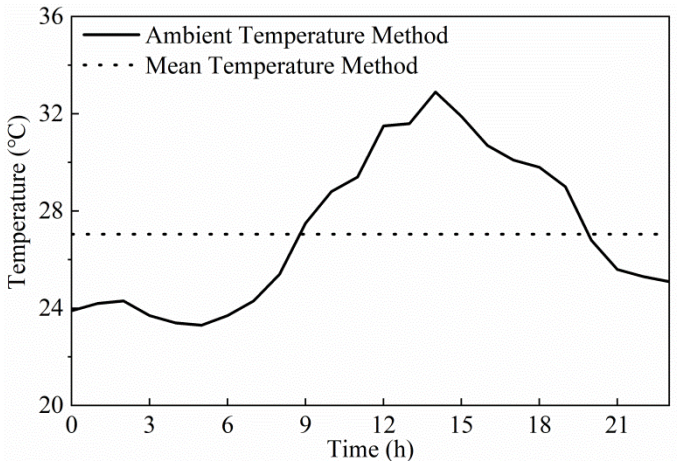

Figure 6. Comparison of different simulation methods for the temperature curves inside the cavities.

2.3. Adjacent Box Girder

One concrete girder with a cross-section consisting of three adjacent box girders in Fuzhou, China was chosen as the case study. The thickness of the Portland cement concrete overlay was 10 cm. The dimensions of the adjacent box girder cross-sections are illustrated in Figure 7. Eight temperature sensors were installed in the top flanges (1-T and 3-T), webs (1-W and 3-W), bottom flanges (1-B and 3-B), and cells (1-C and 3-C) of the adjacent box girders #1 and #3 during the construction process, as shown in Figure 7. Due to space limitations, the data from 24 July 2017 in summer, which is a sunny day with the highest ambient air temperature during the monitoring period, as well as high solar radiation and low wind speed, were selected for analysis. The meteorological data, including ambient air temperature, hourly global solar radiation, hourly diffuse solar radiation,

and wind speed, were measured using a movable automatic meteorological station at the site with a measurement time interval of one hour.

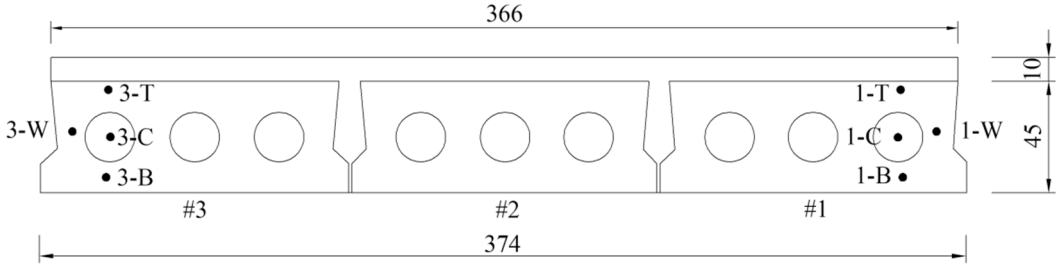

Figure 7. Layout of the adjacent box girder cross-sections (unit: cm).

The midas FEA software was chosen to establish a FEM of the adjacent box girder cross-sections by using two-dimensional plane strain elements, as shown in Figure 8. The four simulation methods for the internal thermal boundary conditions summarized in Section 1 were considered in the FEM of the adjacent box girders. For the Measured Temperature Method, the measured hourly temperature curves inside the cell of the adjacent box girder (24 July 2017) obtained from temperature sensors 1-C and 3-C were chosen, as shown by the hollow points in Figure 9. For the Ambient Temperature Method, the measured hourly ambient air temperature curve (24 July 2017) was used, as shown by the solid line in Figure 9. For the Mean Temperature Method, the mean temperature (35.7 °C) over the previous two days (23 and 24 July 2017) was calculated, as shown by the dashed line in Figure 9. The mesh size of the FEMs using the Measured Temperature Method, Ambient Temperature Method, or Mean Temperature Method was set as 20 mm. The total numbers of nodes and elements were 4,459 and 4,211, respectively, as illustrated in Figure 8a. For the Air Element Method, the total numbers of nodes and elements for the FEM were 4954 and 4868, respectively, as illustrated in Figure 8b. Other detailed information was the same as the FEM of the box girder reported in Section 2.1.

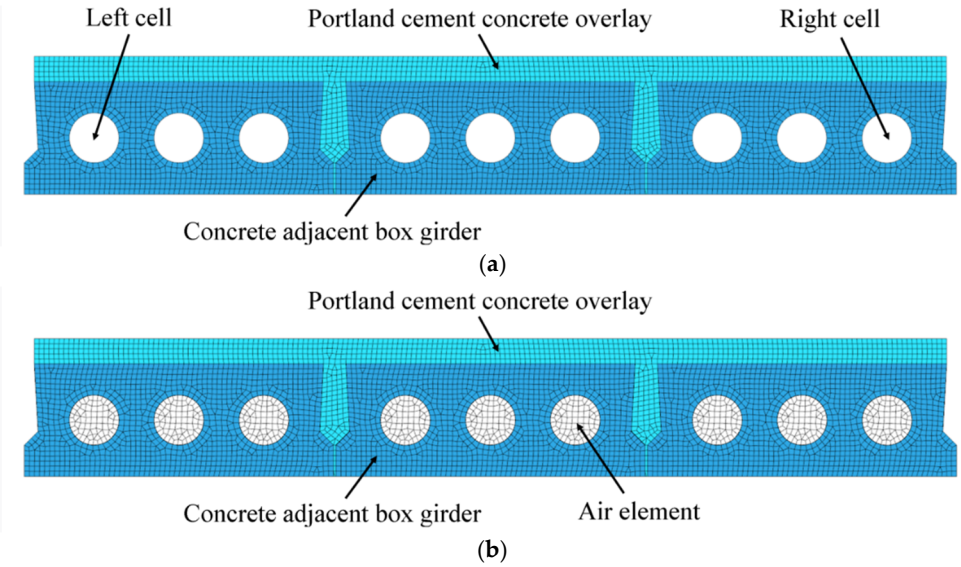

Figure 8. FEM of the adjacent box girder cross-sections: (**a**) FEM without air elements; (**b**) FEM with air elements.

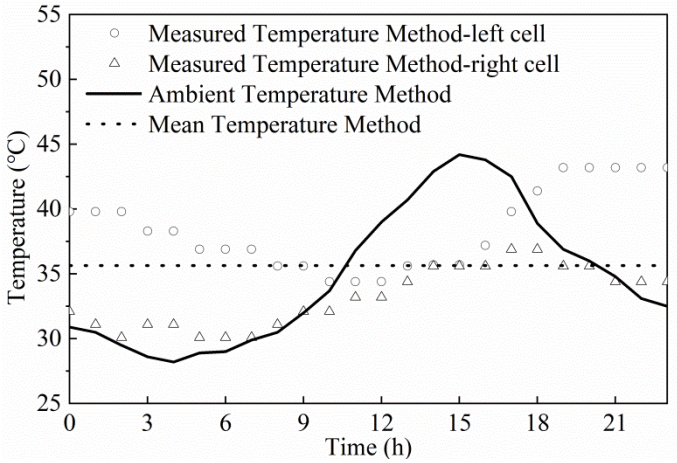

Figure 9. Comparison of different simulation methods for the temperature curves inside the cavities.

3. Influence of Different Simulation Methods for Internal Thermal Boundary Conditions

3.1. Box Girder

3.1.1. Influence on the Hourly Temperature Curves

Due to space limitations, the measured hourly temperature curves obtained from the temperature sensors installed in the right part of the box girder cross-section (T-5, T-4, W-7, W-9, and B-3 as illustrated in Figure 1) were selected for comparison with the numerical hourly temperature curves calculated by the FEMs considering different simulation methods for the internal thermal boundary conditions, as shown in Figure 10. The solid points denote the measured data, and the solid lines with hollow points denote the calculated curves. The root-mean-square error (RMSE) and mean absolute percentage error (MAPE) were used to check the agreement between the measured and calculated temperature curves [49]. The RMSE and MAPE of the numerical hourly temperature curves of the box girder cross-sections obtained from the FEMs with different simulation methods for the internal thermal boundary conditions are illustrated in Figure 11.

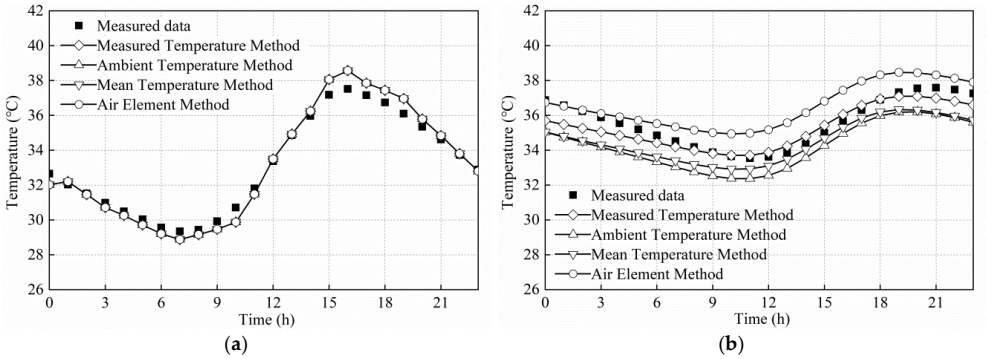

Figure 10. *Cont.*

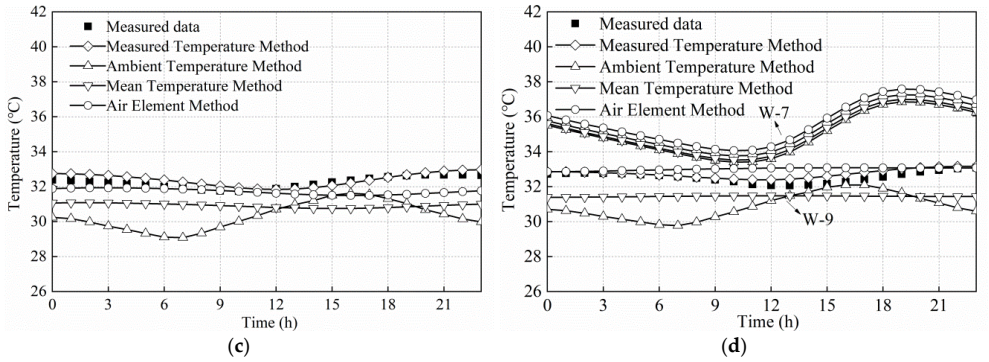

Figure 10. Comparisons of the hourly temperature curves of the box girder cross-sections obtained from the field test and the FEMs with different simulation methods for the internal thermal boundary conditions: (**a**) T-5 in the top flange; (**b**) T-4 in the top flange; (**c**) B-3 in the bottom flange; and (**d**) W-7 and W-9 in the web.

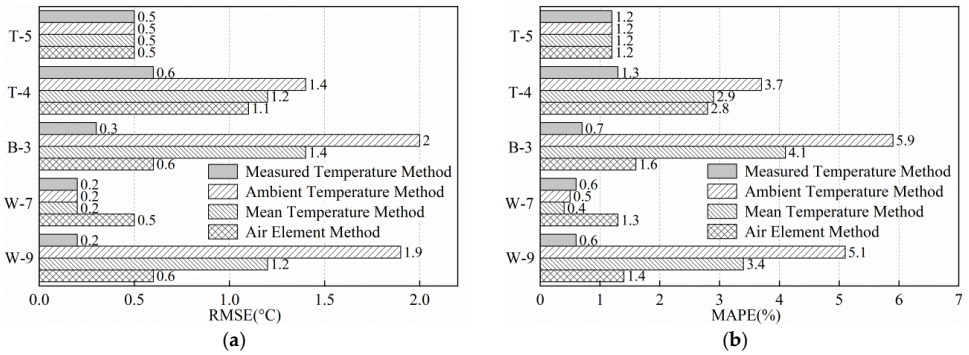

Figure 11. The root-mean-square error (RMSE) and mean absolute percentage error (MAPE) of the numerical hourly temperature curves of the box girder cross-sections obtained from the FEMs with different simulation methods for the internal thermal boundary conditions: (**a**) RMSE; (**b**) MAPE.

In Figures 10a and 11, it can be observed that the influence of the different simulation methods for the internal thermal boundary conditions on the numerical hourly temperature curves of T-5 is negligible. This is because T-5 was in the flange overhang and far from the cavities. Therefore, the temperature distributions on the flange overhangs were not influenced by the internal thermal boundary conditions for the box girder. The RMSE and MAPE in Figure 11 indicate that the differences between the measured and numerical hourly temperature curves were very small (the RMSEs were all 0.5 °C, and the MAPEs were all 1.2%).

In Figure 10b–d, and Figure 11, it can be observed that the trends and the times at which the maximum temperatures occurred are similar for the measured and numerical hourly temperature curves of T-4 and W-7 (which was installed in the web near the top flange). For B-3 and W-9 (which was installed in the web near the bottom flange), it can be observed that the trends for the numerical hourly temperature curves calculated by the Measured Temperature Method, Air Element Method, and Mean Temperature Method are similar to the measured curves. When the Ambient Temperature Method was used, the trends for the numerical curves of B-3 and W-9 are similar to the measured hourly ambient air temperature curve. This is because the temperature change in the hourly ambient air temperature curve was much larger than those in the measured curves inside the cavities. Compared with the measured hourly temperature curves, the numerical curves calculated by the Measured Temperature Method provided the closest agreement (the maximum RMSE was 0.6 °C, and the maximum MAPE was 1.3%). When there is a lack of measured temperatures inside the cavities, the numerical hourly temperature curves calculated by the Air Element Method (the maximum RMSE was 1.1 °C, and the maximum MAPE was 2.8%) provided a closer agreement with the measured curves than the curves calculated by

the Ambient Temperature Method (the maximum RMSE was 2.0 °C, and the maximum MAPE was 5.9%) and the Mean Temperature Method (the maximum RMSE was 1.4 °C, and the maximum MAPE was 4.1%).

The measured hourly temperature curves of all temperature sensors installed in the box girder cross-section were compared with the numerical hourly temperature curves calculated by the FEM using the Air Element Method as the simulation method for the internal thermal boundary condition, as shown in Figure S1. It can be observed that the trends and the times at which the maximum temperatures occurred are similar for the measured hourly temperature curves and numerical curves calculated by the Ambient Temperature Method for all temperature sensors installed in the box girder cross-section (the maximum RMSE was 1.3 °C, and the maximum MAPE was 3.8%).

3.1.2. Influence on the Temperature Contour Plots

The temperature contour plots (15:00, 13 August 2017) obtained from the FEMs considering different simulation methods for the internal thermal boundary conditions are compared in Figure 12. It can be observed that the highest temperature (39.5 °C) was located on the external surfaces of the top flanges and the lowest temperatures (30.3 to 30.7 °C) were located on the undersides of the top and bottom flanges in all FEMs. The influence of different simulation methods for the internal thermal boundary conditions on the highest and lowest temperatures of the box girder cross-section is negligible, because the locations of the highest and lowest temperatures are far from the cavities. The temperature range (32 to 33 °C) was drawn with light blue in Figure 12. The ratio of the light blue area to the total area obtained from the FEM calculated by the Measured Temperature Method was 25.7%, which is larger than the areas calculated by the Ambient Temperature Method (15.4%) and Mean Temperature Method (15.2%) and is smaller than that calculated by the Air Element Method (35.7%). The temperatures on the bottom flange near the cavities calculated by the Measured Temperature Method and Air Element Method were approximately 32 °C, which is close to the measured value (32.3 °C) and larger than the values calculated by the Ambient Temperature Method and Mean Temperature Method (31 °C). It can be concluded that the temperature distributions calculated by the Measured Temperature Method and Air Element Method are similar.

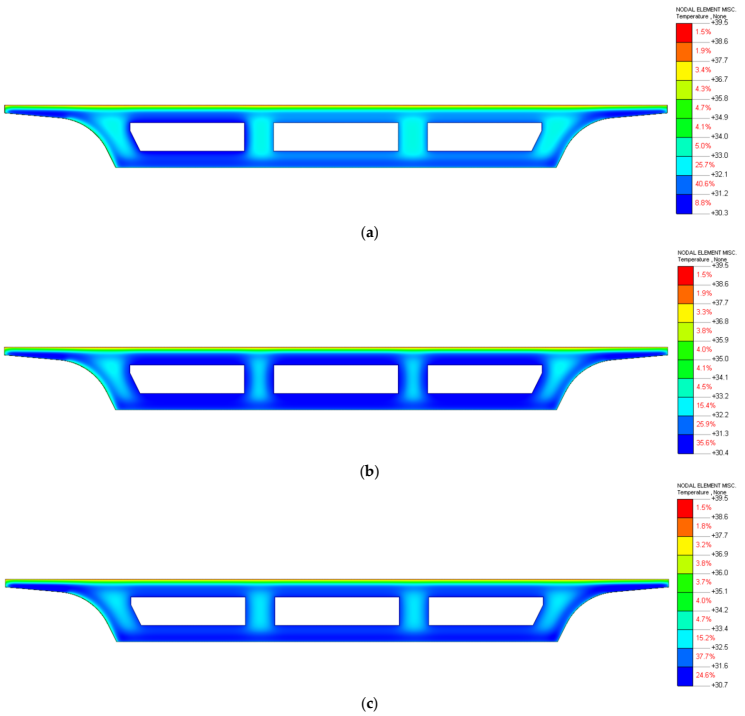

(a)

(b)

(c)

Figure 12. *Cont.*

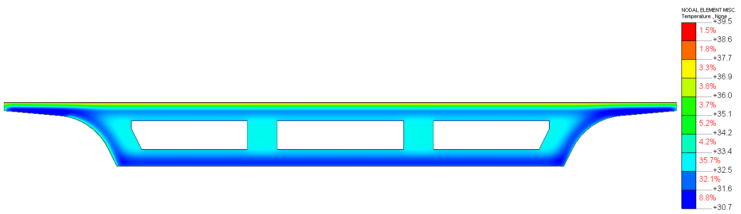

(**d**)

Figure 12. Temperature contour plots of the box girder cross-sections at 15:00 on 13 August 2017: (**a**) Measured Temperature Method; (**b**) Ambient Temperature Method; (**c**) Mean Temperature Method; (**d**) Air Element Method.

3.1.3. Influence on the Average Effective Temperatures and Vertical Temperature Gradients

The hourly average effective temperature (T_{AVG}) of the box girder cross-sections can be estimated using the following rules. The temperature of each element in the FEM is multiplied by its respective element area, and the results for all elements in the cross-section are added together. Then, T_{AVG} can be obtained by dividing the sum by the total area of the cross-section [13,22]. The highest T_{AVG} values of the box girder cross-sections for 13 August 2017, obtained from the field test and the FEMs with different simulation methods for the internal thermal boundary conditions, are listed in Table 1. It can be observed that the influence of different simulation methods for the internal thermal boundary conditions on the highest T_{AVG} was small, with the maximum difference of 0.7 °C.

Table 1. Comparisons of the highest T_{AVG} of the box girder cross-sections obtained from the field test and the FEMs with different simulation methods for the internal thermal boundary conditions (unit: °C).

Methods	Measured Temperature Method	Ambient Temperature Method	Mean Temperature Method	Air Element Method
Measured value		34.9		
Numerical value	35.0	35.0	34.6	35.6

The numerical maximum vertical temperature gradients of the box girder cross-section on 13 August 2017, which were obtained from the FEMs with different simulation methods for the internal thermal boundary conditions, are compared in Figure 13. It can be observed that the influence of different simulation methods for the internal thermal boundary conditions on the trends of the vertical temperature gradients for the box girder cross-section was small, with a maximum difference of 0.4 °C. The maximum vertical temperature differences on the top flanges and bottom flanges calculated by the Ambient Temperature Method and the Mean Temperature Method were slightly larger than those calculated by the Measured Temperature Method and the Air Element Method. The maximum vertical temperature differences on the webs calculated by the Ambient Temperature Method and the Mean Temperature Method were slightly smaller than those calculated by the Measured Temperature Method and the Air Element Method. The numerical maximum vertical temperature gradient of the box girder cross-section calculated by the Air Element Method was close to that calculated by the Measured Temperature Method.

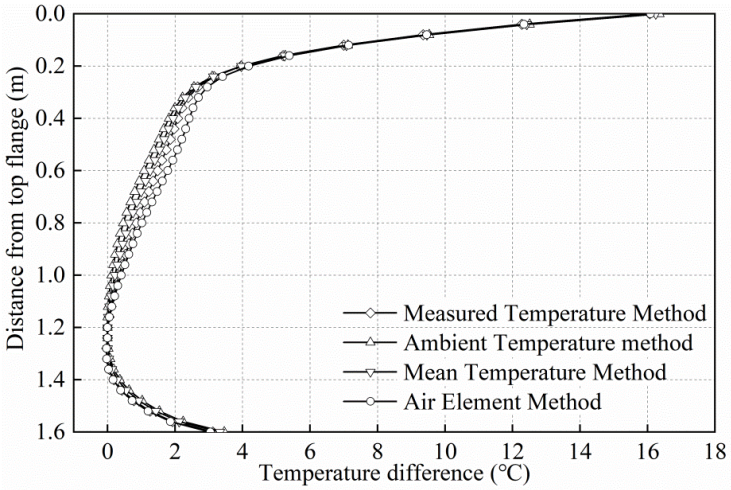

Figure 13. Comparisons of the maximum vertical temperature gradients of the box girder cross-sections obtained from the FEMs with different simulation methods for the internal thermal boundary conditions.

3.2. Small Box Girder

3.2.1. Influence on the Hourly Temperature Curves

Due to space limitations, the measured hourly temperature curves obtained from the temperature sensors installed on the small box girder #7 (7-T, 7-W, and 7-B, as illustrated in Figure 4) were selected for comparison with the numerical hourly temperature curves calculated by the FEMs considering different simulation methods for the internal thermal boundary conditions, as shown in Figure 14. The solid points denote the measured data, and the solid lines with hollow points denote the calculated curves. The RMSE and MAPE of the numerical hourly temperature curves of the small box girder cross-sections obtained from the FEMs with different simulation methods for the internal thermal boundary conditions are illustrated in Figure 15.

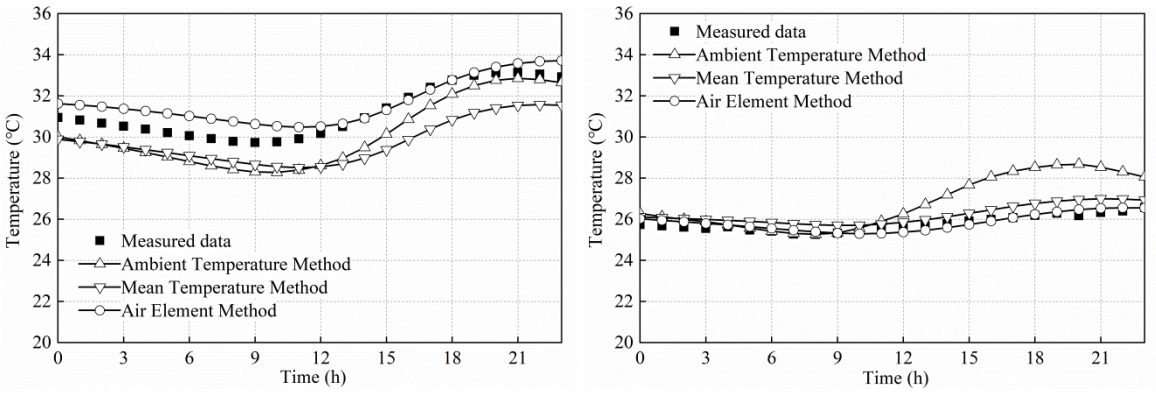

Figure 14. *Cont.*

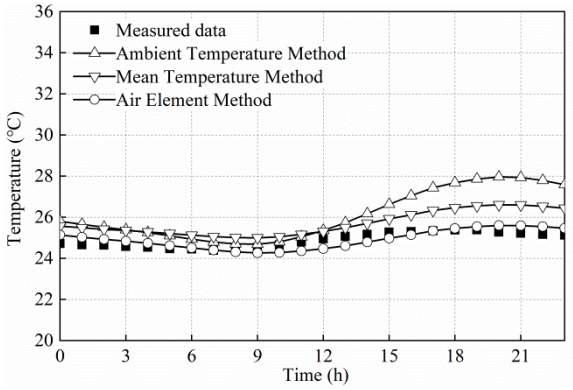

Figure 14. Comparisons of the hourly temperature curves of the small box girder cross-sections obtained from the field test and the FEMs with different simulation methods for the internal thermal boundary conditions: (**a**) 7-T in the top flange; (**b**) 7-W in the web; (**c**) 7-B in the bottom flange.

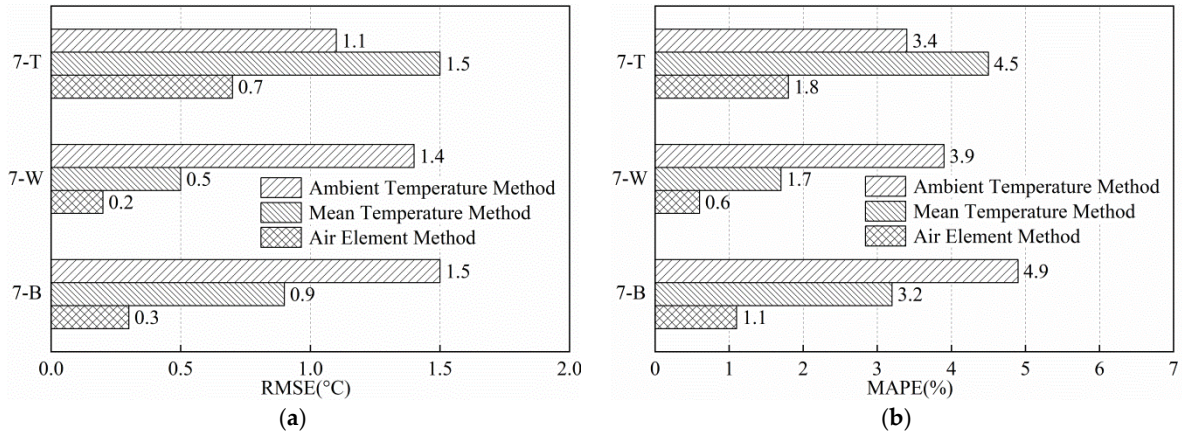

Figure 15. The RMSE and MAPE of the numerical hourly temperature curves of the small box girder cross-sections obtained from the FEMs with different simulation methods for the internal thermal boundary conditions: (**a**) RMSE; (**b**) MAPE.

In Figures 14 and 15, it can be observed that the trends and the times at which the maximum temperatures occurred are similar for the measured and numerical hourly temperature curves of 7-T. For 7-W and 7-B, it can be observed that the trends of the numerical hourly temperature curves calculated by the Air Element Method and Mean Temperature Method are similar to the measured curves. When the Ambient Temperature Method was used, the trends of the numerical curves of 7-W and 7-B are similar to the measured hourly ambient air temperature curve, which is the same as the results for the box girder cross-section. Compared with the measured hourly temperature curves, the numerical hourly temperature curves calculated by the Air Element Method (the maximum RMSE was 0.7 °C, and the maximum MAPE was 1.8%) provided a closer agreement than the curves calculated by the Ambient Temperature Method (the maximum RMSE was 1.5 °C, and the maximum MAPE was 4.9%) and the Mean Temperature Method (the maximum RMSE was 1.5 °C, and the maximum MAPE was 4.5%). In Figure S2, it can be observed that the trends and the times at which the maximum temperatures occurred are similar for the measured hourly temperature curves and numerical curves calculated by the Ambient Temperature Method (the maximum RMSE was 0.8 °C, and the maximum MAPE was 2.6%).

The measured hourly temperature curves of all temperature sensors installed in the small box girder cross-sections were compared with the numerical hourly temperature curves calculated by the FEM using the Air Element Method as the simulation method for the internal thermal boundary

condition, as shown in Figure S2. It can be observed that the trends and the times at which the maximum temperatures occurred are similar for the measured hourly temperature curves and numerical curves calculated by the Ambient Temperature Method for all temperature sensors installed in the small box girder cross-sections (the maximum RMSE was 0.8 °C, and the maximum MAPE was 2.6%).

3.2.2. Influence on the Temperature Contour Plots

The temperature contour plots (15:00, 17 July 2015) obtained from the FEMs considering different simulation methods for the internal thermal boundary conditions are compared in Figure 16. It can be observed that the highest temperature (49.0 °C) was located on the external surfaces of the overlays in all FEMs. The influence of different simulation methods for the internal thermal boundary conditions on the highest temperature of the small box girder cross-sections is negligible because it is far from the cavities. The temperatures of the top flanges (30.8 °C) and bottom flanges (25.9 °C) near the cavities calculated by the Air Element Method were closer to the measured value (31.4 °C for the top flanges and 26.8 °C for the bottom flanges) than those calculated by the Ambient Temperature Method (30.3 °C for the top flanges and 27.4 °C for the bottom flanges) and the Mean Temperature Method (28.3 °C for the top flanges and 25.4 °C for the bottom flanges).

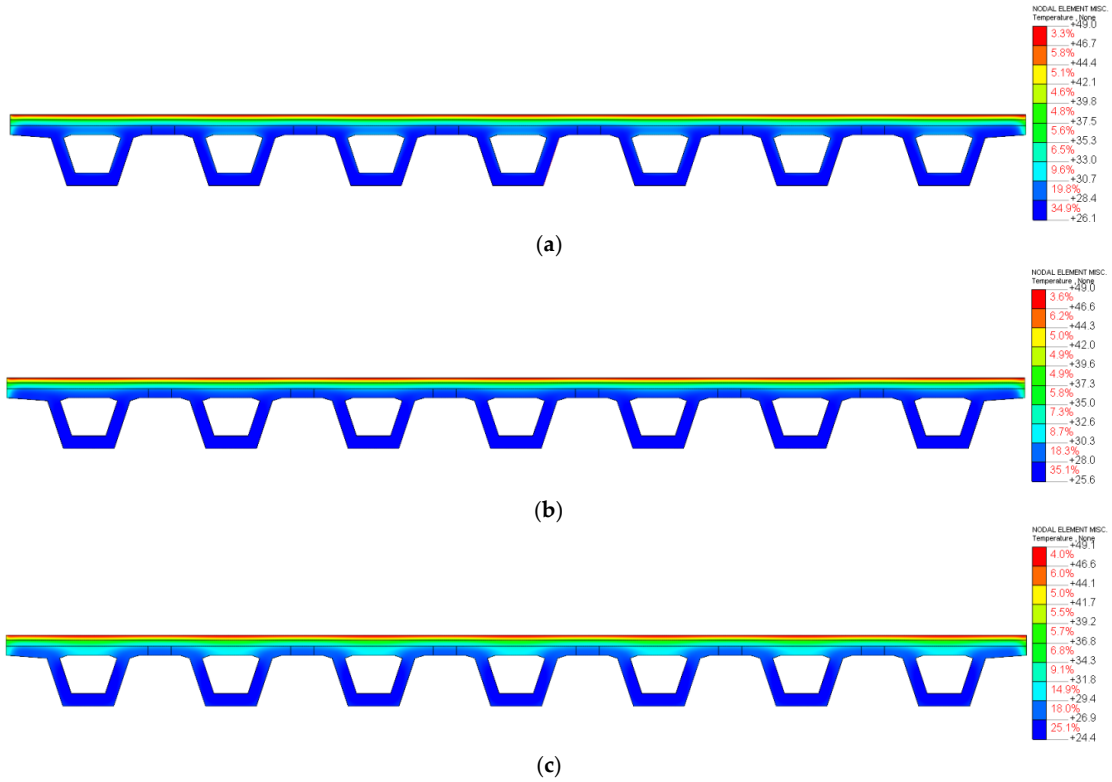

Figure 16. Temperature contour plots of the small box girder cross-sections at 15:00 on 31 July 2014: (**a**) Ambient Temperature Method; (**b**) Mean Temperature Method; (**c**) Air Element Method.

3.2.3. Influence on the Average Effective Temperatures and Vertical Temperature Gradients

The highest T_{AVG} values of the small box girder cross-sections for 17 July, 2015 obtained from the field test and the FEMs with different simulation methods for the internal thermal boundary conditions, are listed in Table 2. It can be observed that the influence of different simulation methods for the internal thermal boundary conditions on the highest T_{AVG} was small, with the maximum difference of 1.1 °C.

Table 2. Comparisons of the highest T_{AVG} of the small box girder cross-sections obtained from the field test and the FEMs with different simulation methods for the internal thermal boundary conditions (Unit: °C).

Methods	Ambient Temperature Method	Mean Temperature Method	Air Element Method
Measured value		28.4	
Numerical value	29.5	28.6	28.6

The numerical maximum vertical temperature gradients of the small box girder cross-sections on 17 July 2015 that were obtained from the FEMs with different simulation methods for the internal thermal boundary conditions are compared in Figure 17. It can be observed that the maximum vertical temperature differences on the top flanges and bottom flanges calculated by the Air Element Method (5.8 °C and 1.5 °C) were larger than those calculated by the Ambient Temperature Method (4.3 °C and 0.8 °C) and the Mean Temperature Method (4.7 °C and 1.1 °C). The influence of different simulation methods for the internal thermal boundary conditions on the vertical temperature difference on the webs was small, with a maximum difference of 0.5 °C.

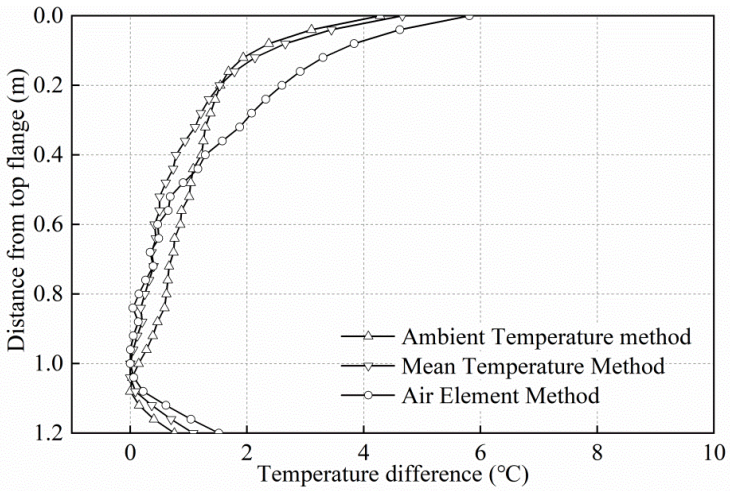

Figure 17. Comparisons of the maximum vertical temperature gradients of the small box girder cross-sections obtained from the FEMs with different simulation methods for the internal thermal boundary conditions.

3.3. Adjacent Box Girder

3.3.1. Influence on the Hourly Temperature Curves

Due to space limitations, the measured hourly temperature curves obtained from the temperature sensors installed on the adjacent box girder #3 (3-T, 3-W, and 3-B as illustrated in Figure 7) were selected for comparison with the numerical hourly temperature curves calculated by the FEMs considering different simulation methods for the internal thermal boundary conditions, as shown in Figure 18. The solid points denote the measured data, and the solid lines with hollow points denote the calculated curves. The RMSE and MAPE of the numerical hourly temperature curves of the adjacent box girder cross-sections obtained from the FEMs with different simulation methods for the internal thermal boundary conditions are illustrated in Figure 19.

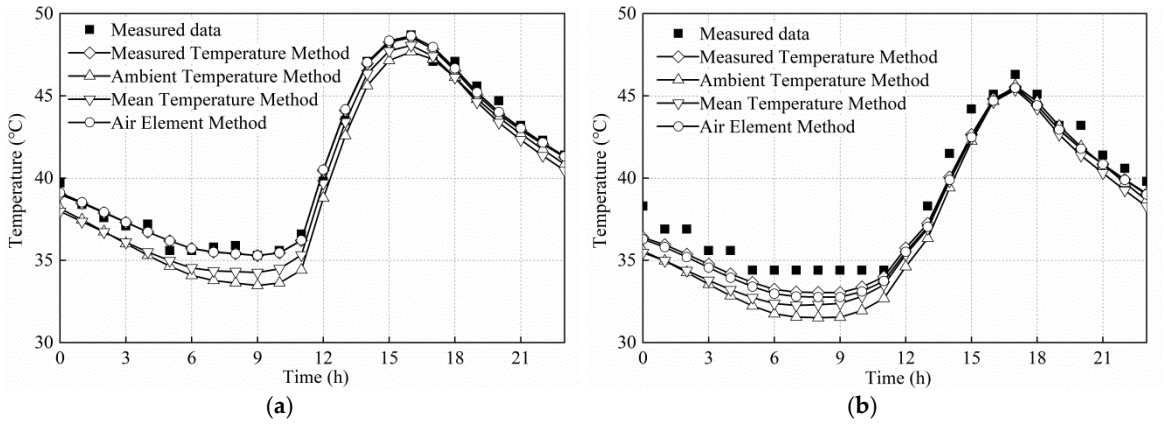

Figure 18. *Cont.*

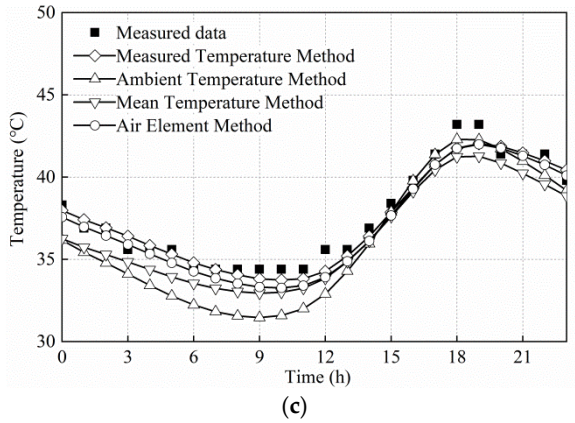

Figure 18. Comparisons of the hourly temperature curves of the adjacent box girder cross-sections obtained from the field test and the FEMs with different simulation methods for the internal thermal boundary conditions: (**a**) 3-T in the top flange; (**b**) 3-W in the web; (**c**) 3-B in the bottom flange.

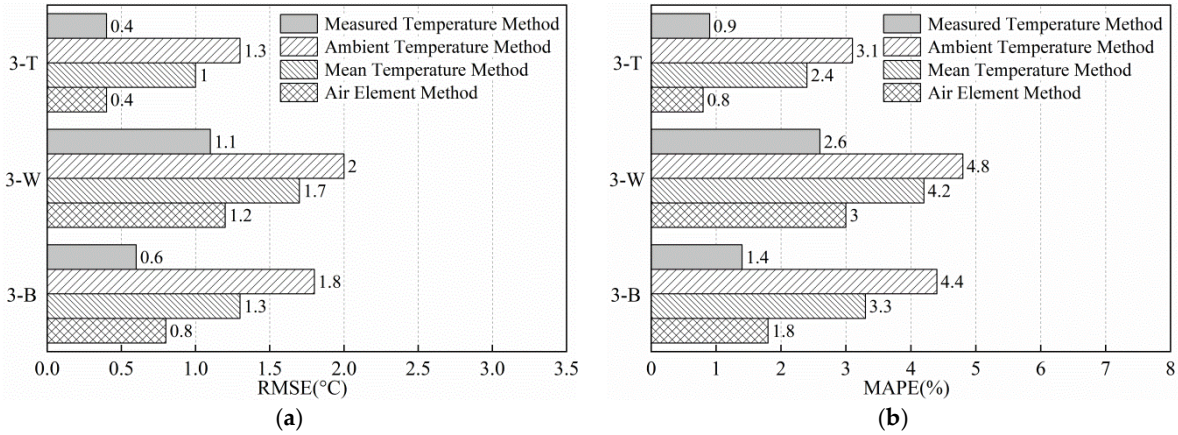

Figure 19. The RMSE and MAPE of the numerical hourly temperature curves of the adjacent box girder cross-sections obtained from the FEMs with different simulation methods for the internal thermal boundary conditions: (**a**) RMSE; (**b**) MAPE.

In Figures 18 and 19, it can be observed that the trends and the times at which the maximum temperatures occurred are similar for the measured and numerical hourly temperature curves of 3-T, 3-W, and 3-B. The influence of the Ambient Temperature Method on the trends of the numerical

hourly temperature curves of the bottom flanges on the adjacent box girders is much smaller than that on the box girder or small box girders. This is because the area of the cavities in the adjacent box girders illustrated in Figure 7 is quite small. Compared with the measured hourly temperature curves, the numerical curves calculated by the Measured Temperature Method (the maximum RMSE was 1.1 °C, and the maximum MAPE was 2.6%) and the Air Element Method (the maximum RMSE was 1.2 °C, and the maximum MAPE was 3.0%) provided the closest agreement. When there is a lack of measured temperatures inside the cavities, the numerical hourly temperature curves calculated by the Air Element Method provided a closer agreement with the measured curves than the curves calculated by the Ambient Temperature Method (the maximum RMSE was 2.0 °C, and the maximum MAPE was 4.8%) and the Mean Temperature Method (the maximum RMSE was 1.7 °C, and the maximum MAPE was 4.2%).

The measured hourly temperature curves of all temperature sensors installed in the adjacent box girder cross-sections were compared with the numerical hourly temperature curves calculated by the FEM using the Air Element Method as the simulation method for the internal thermal boundary condition, as shown in Figure S3. It can be observed that the trends and the times at which the maximum temperatures occurred are similar for the measured hourly temperature curves and numerical curves calculated by the Ambient Temperature Method for all temperature sensors installed in the adjacent box girder cross-sections (the maximum RMSE was 1.2 °C, and the maximum MAPE was 3.0%).

3.3.2. Influence on the Temperature Contour Plots

The temperature contour plots (15:00, 24 July 2017) obtained from the FEMs considering different simulation methods for the internal thermal boundary conditions are compared in Figure 20. It can be observed that the influence of different simulation methods for the internal thermal boundary conditions on the adjacent girder #1 is negligible because girder #1 was covered by a shadow. The highest temperature (57.8 °C) was located on the external surface of the top flange in girder #3, which was exposed to sunlight in all the FEMs. The influence of different simulation methods for the internal thermal boundary conditions on the highest temperature of the adjacent box girder cross-section is negligible because it is far from the cavities. The temperature distributions on the adjacent box girder cross-sections calculated by the Measured Temperature Method and Air Element Method were similar and smaller than those calculated by the Ambient Temperature Method and larger than those calculated by the Mean Temperature Method.

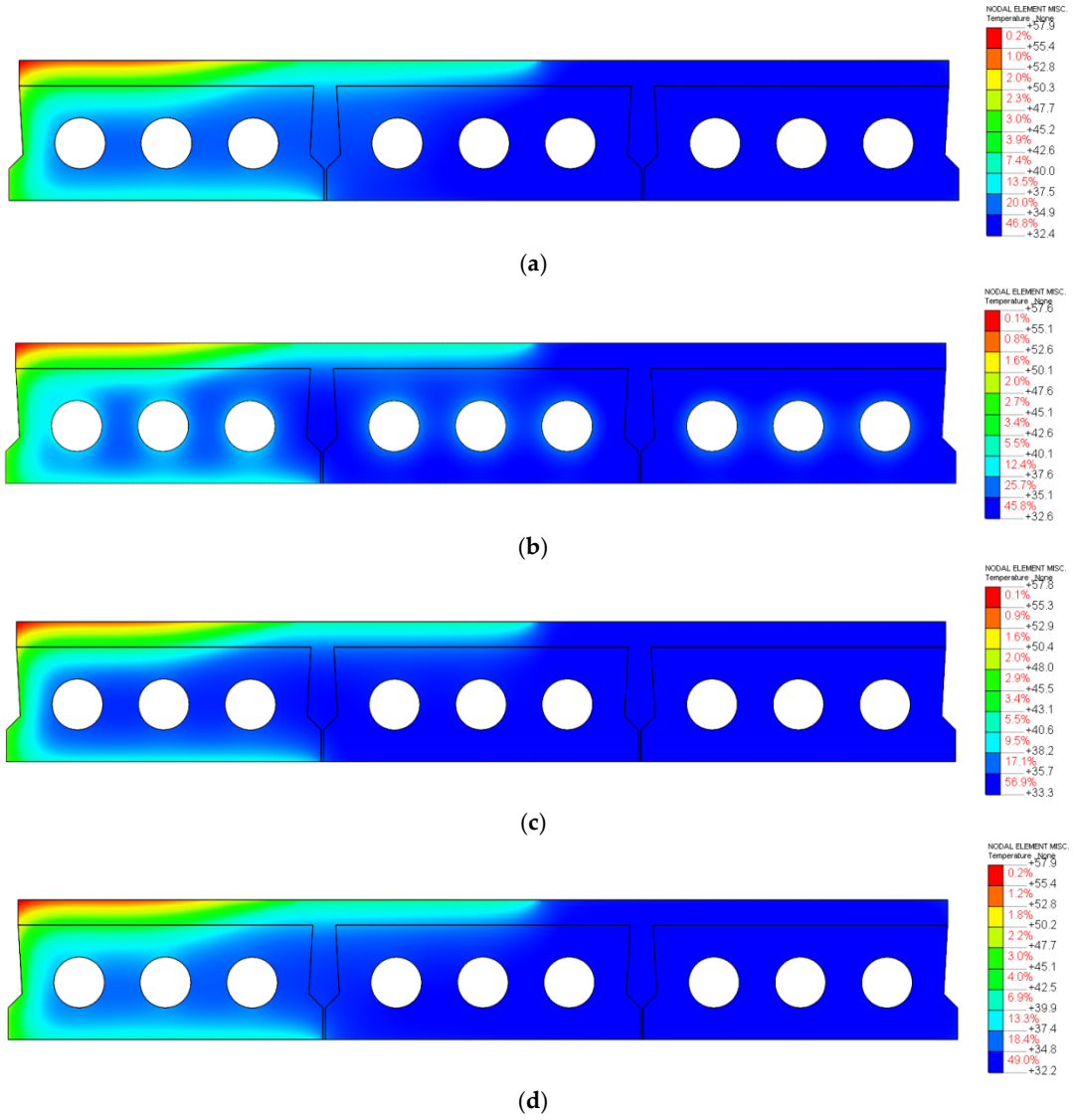

Figure 20. Temperature contour plots of the adjacent box girder cross-sections at 15:00 on 24 July 2017: (**a**) Measured Temperature Method; (**b**) Ambient Temperature Method; (**c**) Mean Temperature Method; (**d**) Air Element Method.

3.3.3. Influence on the Average Effective Temperatures and Vertical Temperature Gradients

The highest T_{AVG} values of the adjacent box girder cross-sections for 24 July 2017 obtained from the field test and the FEMs with different simulation methods for the internal thermal boundary conditions are listed in Table 3. It can be observed that the influence of different simulation methods for the internal thermal boundary conditions on the highest T_{AVG} was small, with a maximum difference of 0.8 °C.

Table 3. Comparisons of the highest T_{AVG} of the adjacent box girder cross-sections obtained from the field test and the FEMs with different simulation methods for the internal thermal boundary conditions (Unit: °C).

Methods	Measured Temperature Method	Ambient Temperature Method	Mean Temperature Method	Air Element Method
Measured value		37.5		
Numerical value	37.0	37.8	37.1	36.7

The numerical maximum vertical temperature gradients of the adjacent box girder cross-sections on 24 July 2017, obtained from the FEMs with different simulation methods for the internal thermal boundary conditions are compared in Figure 21. It can be observed that the influence of different simulation methods for the internal thermal boundary conditions on the trends of the vertical temperature gradients for the adjacent box girder cross-sections was small, with a maximum difference of 0.5 °C. The maximum vertical temperature differences on the top flanges and bottom flanges calculated by the Ambient Temperature Method were slightly smaller than those calculated by the other three methods. The maximum vertical temperature differences on the webs calculated by different simulation methods for the internal thermal boundary conditions were almost the same.

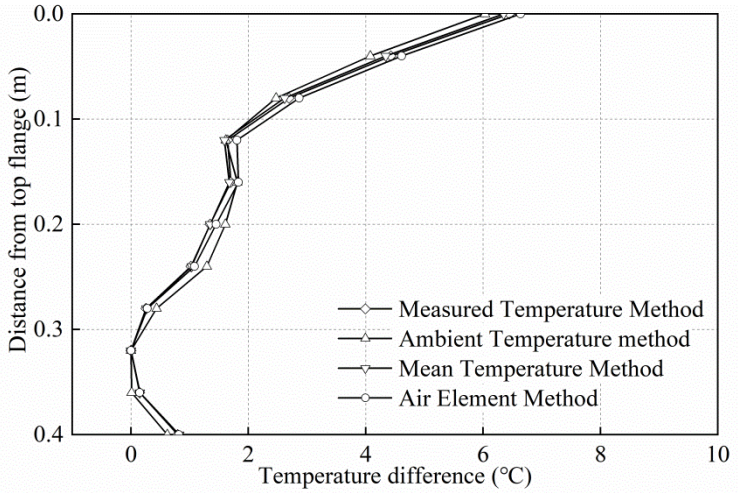

Figure 21. Comparisons of the maximum vertical temperature gradients of the adjacent box girder cross-sections obtained from the FEMs with different simulation methods for the internal thermal boundary conditions.

4. Temperature Distributions on Concrete Closed Girder Cross-Sections under Historically Extreme Temperature Conditions

The temperature curves inside the cavities under historically extreme temperature conditions are difficult to measure. However, the Air Element Method can be used as a simulation method for the internal thermal boundary conditions in the FEM to predict the temperature distributions on concrete closed girder cross-sections under historically extreme temperature conditions.

4.1. Meteorological Data

In order to simulate the external thermal boundary conditions in the FEMs, the hourly ambient air temperature curves, hourly solar radiation curves, and wind speed under historically extreme temperature conditions should be assumed. The sinusoidal function was used to simulate the hourly

ambient air temperature curves by determining the maximum and minimum ambient air temperatures (T_{max} and T_{min}) using the following Equation [15]:

$$T_i = a\sin\omega_i + \beta \quad (2)$$

where T_i is the ambient air temperature at the ith hour, a and β are the model coefficients calculated by $a = (T_{max} - T_{min})/2$ and $\beta = (T_{max} + T_{min})/2$, and ω_i is the hour angle at the ith hour.

The designed life of a highway bridge is set at 100 years, according to the Chinese code (JTG D60-2015) [50]. Based on the historical extreme temperatures obtained from the China Meteorological Administration [51] and an assumption of a normal distribution with a confidence of 95% [52], the T_{max} and T_{min} for the 100-year return period can be predicted, as listed in Table 4. The monthly average daily temperature range can be obtained from the China Meteorological Administration [51]. The idealized hourly temperature curve on the hottest day was based on T_{max}, and the corresponding lowest temperature of the idealized curve was selected by subtracting the monthly average daily temperature range in July. The idealized hourly temperature curve on the coldest day was based on T_{min}, and the corresponding highest temperature of the idealized curve was selected by adding the monthly average daily temperature range in January [13,53]. The times at which T_{max} and T_{min} occurred in the idealized hourly temperature curves under historically extreme temperature conditions were assumed to be 14:00 for the idealized hourly temperature curve on the hottest day and 06:00 for the idealized hourly temperature curve on the coldest day. According to the bridge locations introduced in Chapter 2, the hourly ambient air temperature curves (continued for five days) under historically extreme temperature conditions in Shenzhen, Handan, and Fuzhou are illustrated in Figure 22.

Table 4. Meteorological parameters of the hourly ambient air temperature curves under historically extreme temperature conditions (Unit: °C).

Cross-Section	Location	Ambient Air Temperature		Monthly Average Daily Temperature Range	
		Max	Min	July	January
Box girder	Shenzhen	37.9	−0.3	6.1	7.4
Small box girder	Handan	43.1	−21.3	8.9	8.9
Adjacent box girder	Fuzhou	40.6	−1.9	8.7	7.0

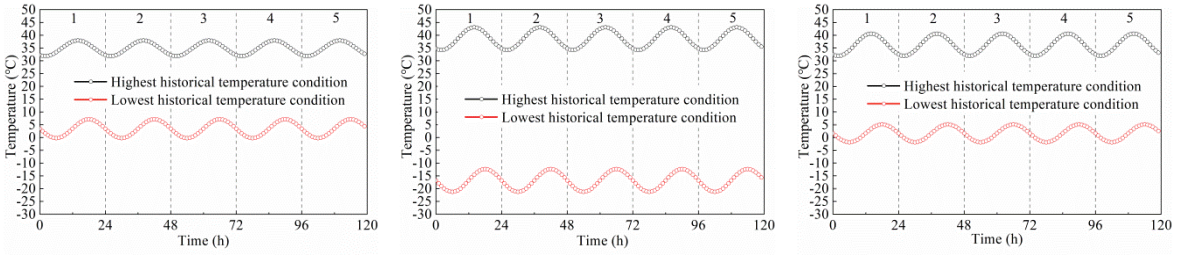

Figure 22. Idealized hourly ambient air temperature curves under historically extreme temperature conditions: (**a**) Shenzhen; (**b**) Handan; (**c**) Fuzhou.

Under the highest historical temperature condition, the yearly maximum hourly solar radiation occurs on 21 June, which has the maximum sunshine duration and extraterrestrial radiation [54]. The hourly beam solar radiation and diffuse solar radiation on 21 June can be simulated by using numerical models [25] based on the solar radiation data obtain from the National Aeronautics and

Space Administration (NASA) Langley Research Center [55], as illustrated in Figure 23. Under the lowest historical temperature condition, the influence of solar radiation was not considered.

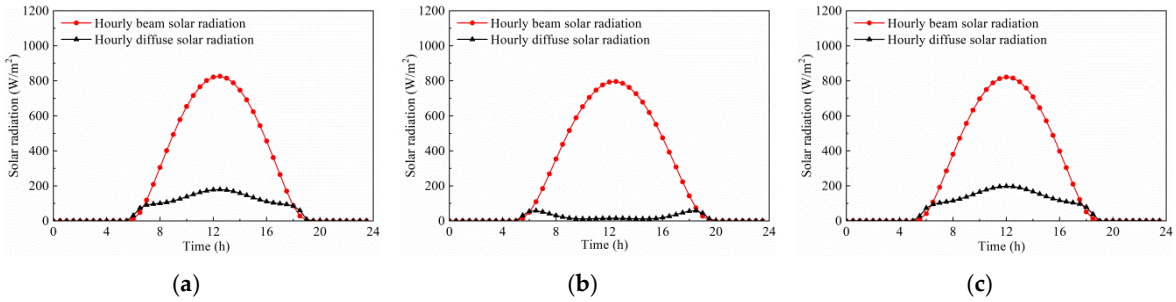

Figure 23. Numerical hourly beam solar radiation and diffuse solar radiation under the highest historical temperature conditions: (**a**) Shenzhen; (**b**) Handan; (**c**) Fuzhou.

The smaller the wind speed, the higher the temperature of the girder cross-section [17]. However, the probability that zero wind speed and the maximum temperature will occur together is extremely small. A wind speed of 1.0 m/s [14,56] was used to analyze the temperature of the concrete bridge structure under the highest historical temperature conditions. The maximum basic wind speeds for the 100-year return period, which is 37.5 m/s for Shenzhen, 27.9 m/s for Handan, and 34.0 m/s for Fuzhou [57], were chosen as the wind speeds under the lowest historical temperature conditions.

In order to reduce the influence of the initial thermal boundary condition, the same idealized hourly ambient air temperature curves, hourly solar radiation curves, and wind speed were imposed cyclically for five days.

4.2. *Average Effective Temperatures of Cross-Sections*

Based on the aforementioned meteorological data under historically extreme temperature conditions and the Air Element Method, the FEMs of the concrete closed girder cross-sections were established to predict the peak average effective temperatures of the cross-sections under historically extreme temperature conditions (hereafter referred to as T_E). The one-year measured average effective temperatures of the cross-sections can be obtained from the field test (hereafter referred to as T_M). The maximum and minimum effective temperatures of highway concrete bridges were recommended by the Chinese code JTG D60-2015 [50] (hereafter referred to as T_C). China is partitioned into four climatic regions that are categorized as severe cold, cold, warm, and "other" regions [50]. Handan is in the cold region, with the highest T_C of 34 °C and the lowest T_C of −10 °C; Shenzhen is in the warm region, with the highest T_C of 34 °C and the lowest T_C of −3 °C; and Fuzhou is in the "other" region, with the highest T_C of 34 °C and the lowest T_C of 0 °C. Comparisons of T_M, T_C, and T_E are illustrated in Figure 24.

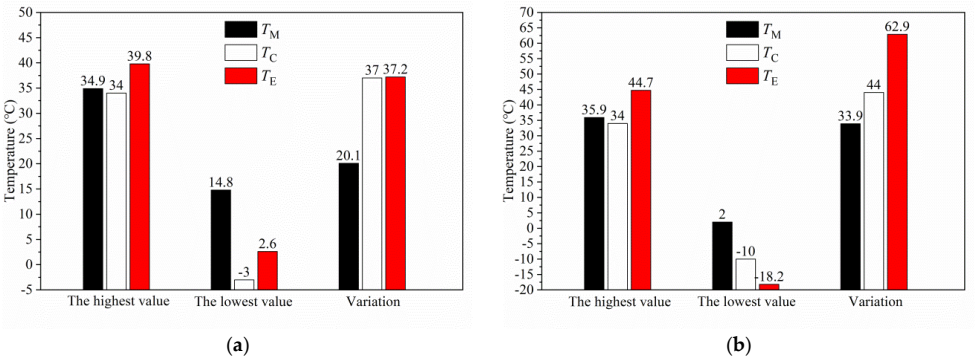

Figure 24. *Cont.*

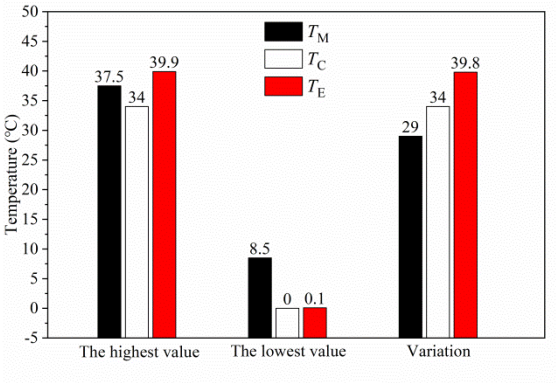

(**c**)

Figure 24. Comparisons of T_M, T_C, and T_E: (**a**) Box girder cross-section; (**b**) small box girder cross-sections; (**c**) adjacent box girder cross-sections.

The comparisons of T_M, T_C, and T_E for the box girder cross-section are illustrated in Figure 24a. It can be observed that the highest T_M was close to the highest T_C (a difference of 0.9 °C), and these values were lower than the highest T_E (differences of 4.9 °C for T_M and 5.8 °C for T_C). The lowest T_M was much higher than the lowest T_E (a difference of 12.2 °C) and the lowest T_C (a difference of 17.8 °C). The variation of T_C was close to that of T_E (a difference of only 0.2 °C), and they were larger than that of T_M (differences of 16.9 °C for T_C and 17.1 °C for T_E). It can be predicted that the longitudinal thermal movement of the concrete box girder under historically extreme temperature conditions would be underestimated by considering the variation of T_M. The variations of T_C (37.0 °C) and T_E (37.2 °C) were almost the same. However, assuming that the datum temperatures (T_0) were the same, the thermal expansion of the concrete box girder calculated by the difference between the highest T_C and T_0 would be smaller than that calculated by the difference between the highest T_E and T_0, while the thermal contraction of the concrete box girder calculated by the difference between T_0 and the lowest T_C would be larger than that calculated by the difference between T_0 and the lowest T_E.

The comparisons of T_M, T_C, and T_E for the small box girder cross-sections are illustrated in Figure 24b. It can be observed that the highest T_E (44.7 °C) was significantly higher than the highest T_M (a difference of 8.8 °C) and the highest T_C (a difference of 10.7 °C); meanwhile, the lowest T_E (−18.2 °C) was significantly lower than the lowest T_M (a difference of 20.2 °C) and the lowest T_C (a difference of 8.2 °C). The variation of T_E (62.9 °C) was significantly larger than that of T_M (a difference of 29.0 °C) and T_C (a difference of 18.9 °C), which was possibly because Handan is in Northern China, where the variation of ambient air temperature is large. It can be predicted that the longitudinal thermal movement of the concrete small box girders under historically extreme temperature conditions would be underestimated by considering variations of T_M or T_C.

The comparisons of T_M, T_C, and T_E for the adjacent box girder cross-sections are illustrated in Figure 24c. It can be observed that the highest T_E (39.8 °C) was higher than the highest T_M (a difference of 4.9 °C) and the highest T_C (a difference of 5.8 °C); meanwhile, the lowest T_E (0.1 °C) was lower than the lowest T_M (a difference of 8.4 °C) and similar to the lowest T_C (a difference of only 0.1 °C). The variation of T_E (39.8 °C) was larger than that of T_M (a difference of 10.8 °C) and T_C (a difference of 5.8 °C). It can be predicted that the longitudinal thermal movement of the concrete adjacent box girders under historically extreme temperature conditions would be underestimated by considering variations of T_M or T_C.

Therefore, it can be concluded that the longitudinal thermal movement of the concrete closed girders calculated by the one-year measured average effective temperature of cross-sections or by the Chinese-code-specified effective temperatures for highway bridge structures is smaller than that under historically extreme temperature conditions, which are thus unconservative for engineering applications. It is suggested that the average effective temperature for the concrete closed girder

cross-sections under historically extreme temperature conditions should be calculated for each city using the FEM with the Air Element Method described in this paper.

4.3. Vertical Temperature Gradients

Based on the aforementioned meteorological data under historically extreme temperature conditions and the Air Element Method, the FEMs of the concrete closed girder cross-sections were established to predict the vertical temperature gradients under historically extreme temperature conditions. The highest temperatures for the bridge deck surface proposed by Chinese code JTG D60-2015 [50] are 25 °C for Portland cement concrete overlays and 14 °C for 100 mm asphalt concrete overlays (for positive vertical temperature differences), and the lowest temperatures of the bridge deck surface are −12.5 °C for Portland cement concrete overlays and −7 °C for 100 mm asphalt concrete overlays (for negative vertical temperature differences). The numerical vertical temperature gradients of cross-sections under historically extreme temperature conditions and the designed vertical temperature gradients for concrete superstructures proposed by Chinese code JTG D60-2015 [50] are compared in Figures 25–27.

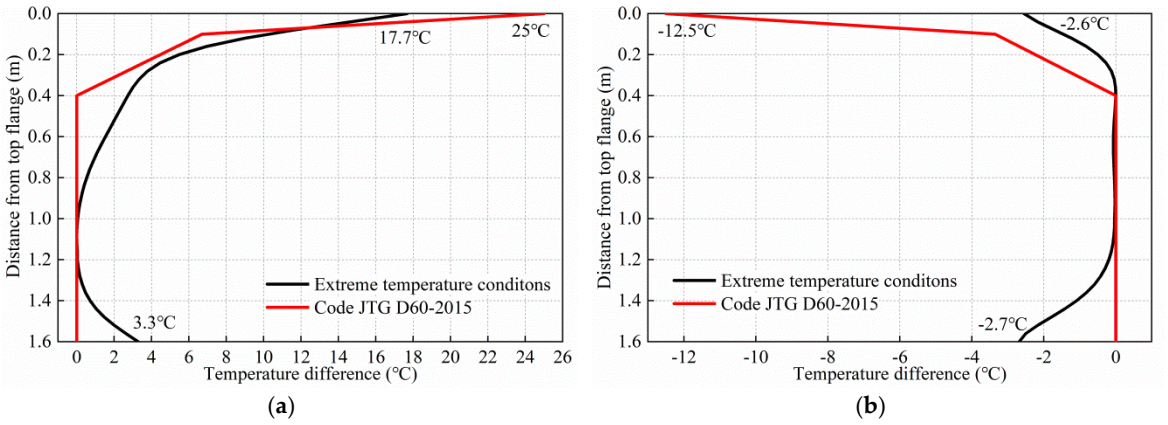

Figure 25. Comparison of the vertical temperature gradients of the box girder cross-section: (**a**) Positive vertical temperature gradient; (**b**) negative vertical temperature gradient.

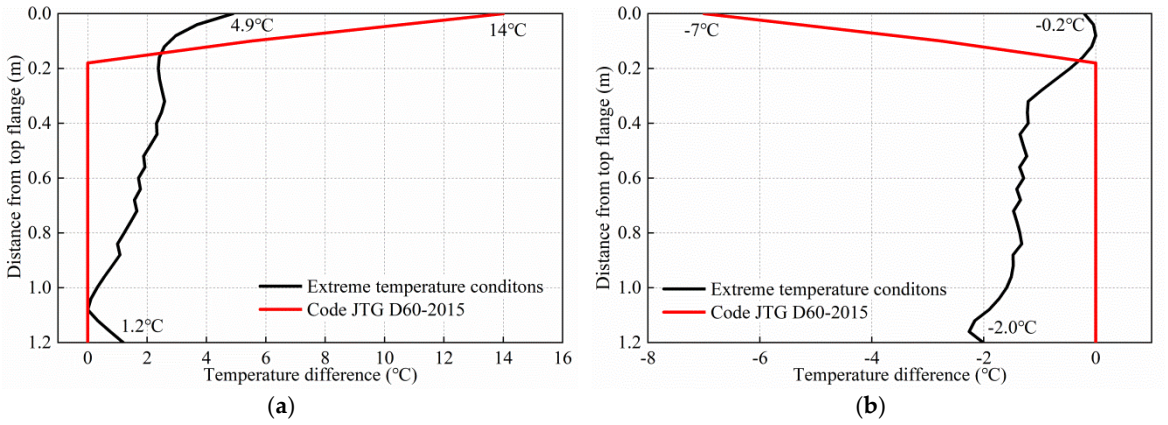

Figure 26. Comparison of the vertical temperature gradients of the small box girder cross-sections: (**a**) Positive vertical temperature gradient; (**b**) negative vertical temperature gradient.

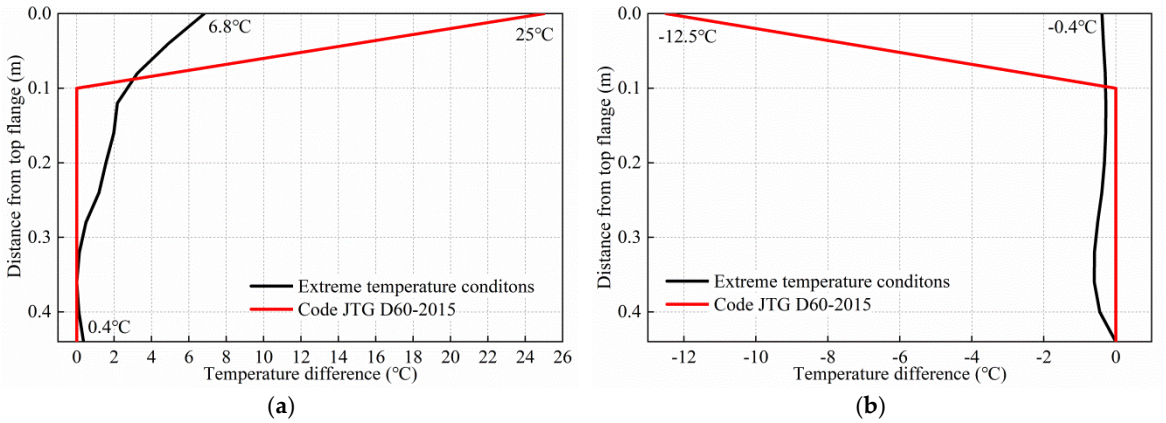

Figure 27. Comparison of the vertical temperature gradients of the adjacent box girder cross-sections: (**a**) Positive vertical temperature gradient; (**b**) negative vertical temperature gradient.

For positive vertical temperature differences, the designed highest temperatures of the bridge deck surface were higher than those obtained from the FEMs with differences of 7.3 °C for the box girder cross-section, 9.1 °C for the small box girder cross-sections, and 18.2 °C for the adjacent box girder cross-sections, respectively. For negative vertical temperature differences, the designed lowest temperatures of the bridge deck surface were lower than those obtained from the FEMs with differences of 9.9 °C for the box girder cross-section, 6.8 °C for the small box girder cross-sections, and 12.1 °C for the adjacent box girder cross-sections, respectively. Therefore, it can be concluded that the Chinese-code-specified design temperatures of the bridge deck surfaces in vertical temperature gradients are conservative.

The temperature differences on the bottom flanges were not considered in Chinese code JTG D60-2015 [50]. However, the extreme temperature differences on the bottom flanges under historically extreme temperature conditions obtained from the FEMs were 3.3 °C and −2.7 °C for the box girder cross-section, and 1.2 °C and −2.0 °C for the small box girder cross-sections, respectively. The temperature differences on the bottom flanges of the adjacent box girder cross-sections are negligible because the bottom flange height of the adjacent box girders is small (0.44 m). Therefore, it can be concluded that the Chinese-code-specified design temperatures on the bottom flanges in the vertical temperature gradients are unconservative.

5. Summary

The following conclusions can be drawn based on the results, and within the limitations, of the research presented in this paper:

(1) The Measured Temperature Method can reflect the actual temperatures inside the cavities, but measurements on site are cost- and time-prohibitive. Therefore, the application range of the Measured Temperature Method is limited. When there is no measurement on site to obtain the temperature inside the cavity, the Ambient Temperature Method, Mean Temperature Method, or Air Element Method can be used as alternative methods.

(2) The influences of different simulation methods for the internal thermal boundary conditions on the numerical hourly temperature curves of the parts of cross-sections far from the cavities are negligible. Compared with the measured hourly temperature curves, the numerical hourly temperature curves of the parts of the cross-sections near the cavities calculated by the Measured Temperature Method provide the closest agreement. When there is a lack of measured temperature inside the cavity, the numerical hourly temperature curves calculated by the Air Element Method provide a closer agreement with the measured curves than the curves calculated by the Ambient Temperature Method and Mean Temperature Method. When the Ambient Temperature Method is used, the trends of the numerical curves of the bottom flanges and the webs near the bottom

flanges are similar to the measured hourly ambient air temperature curve, because the temperature change in the hourly ambient air temperature curve was much larger than the temperature changes in the measured curves inside the cavities.

(3) The comparisons of the temperature contour plots obtained from the FEMs considering different simulation methods for the internal thermal boundary conditions indicated that the temperature distributions on the parts near the cavities calculated by the Measured Temperature Method and Air Element Method were close to the measured values.

(4) The influences of different simulation methods for the internal thermal boundary conditions on the highest hourly average effective temperature of concrete closed girder cross-sections and the trends of the vertical temperature gradients for the box girder and adjacent box girder cross-sections were small. The maximum vertical temperature gradients calculated by the Air Element Method on the top and bottom flanges were larger than those calculated by the Ambient Temperature Method and Mean Temperature Method for the small box girder cross-sections.

(5) The Air Element Method can be used as a simulation method for the internal thermal boundary conditions in the FEM to predict the temperature distributions on concrete closed girder cross-sections under historically extreme temperature conditions. The longitudinal thermal movement of concrete closed girders calculated by the one-year measured average effective temperature of the cross-sections or by the Chinese-code-specified effective temperatures for the highway bridge structures would be smaller than those under historically extreme temperature conditions, which are thus unconservative for engineering applications. It is suggested that the average effective temperature of concrete closed girder cross-sections under historically extreme temperature conditions should be calculated for each city using the FEM with the Air Element Method, as described in this paper. The comparisons of vertical temperature gradients under historically extreme temperature conditions indicate that the Chinese-code-specified vertical temperature gradients are conservative for the bridge deck surfaces and unconservative for the bottom flanges.

(6) Further research has been carried out to analyze the average effective temperatures and vertical temperature gradients of concrete closed girder cross-sections under historically extreme temperature conditions for each city in China using the FEM with the Air Element Method described in this paper.

Supplementary Materials: The following are available online at http://www.mdpi.com/2076-3417/10/4/1274/s1, Figure S1: Comparisons of the hourly temperature curves of the box girder cross-sections obtained by the field test and the FEM using the Air Element Method as the simulation method for the internal thermal boundary conditions: (a) Sensors in the top flange; (b) sensors in the bottom flange; (c) sensors in the left exterior web; (d) sensors in the interior webs; (e) sensors in the right exterior web, Figure S2: Comparisons of the hourly temperature curves of the small box girder cross-sections obtained by the field test and the FEM using the Air Element Method as the simulation method for the internal thermal boundary conditions: (a) Sensors in the top flanges; (b) sensors in the bottom flanges; (c) sensors in the webs, Figure S3: Comparisons of the hourly temperature curves of the adjacent box girder cross-sections obtained by the field test and the FEMs using the Air Element Method as the simulation method for the internal thermal boundary conditions: (a) Sensors in the top flanges; (b) sensors in the bottom flanges; (c) sensors in the webs.

Author Contributions: Conceptualization, J.X.; Data curation, J.L. and J.X.; Funding acquisition, J.X. and F.H.; Investigation, J.L., J.X., and B.C.; Software, J.L., J.X., and F.H.; Writing—original draft, J.L.; Writing—review and editing, J.X., F.H., and B.C. All authors have read and agreed to the published version of the manuscript.

Funding: This research was funded by the National Natural Science Foundation of China grant number 51508103 and the National Natural Science Foundation of China 51578161.

Acknowledgments: The authors would also like to acknowledge the National Meteorological Information Center, China Meteorological Administration.

Conflicts of Interest: The authors declare no conflict of interest.

References

1. Lall, J.; Alampalli, S.; DiCocco, E.F. Performance of full depth shear keys in adjacent prestressed box beam bridges. *PCI J.* **1998**, *43*, 72–79. [CrossRef]
2. Miller, R.A.; Hlavacs, G.M.; Long, T.; Greuel, A. Full-scale testing of shear keys for adjacent box girder bridges. *PCI J.* **1999**, *44*, 80–90. [CrossRef]
3. Sennah, K.M.; Kennedy, J.B. Literature review in analysis of box-girder bridges. *J. Bridge Eng.* **2002**, *7*, 134–143. [CrossRef]
4. Russell, H.G. Adjacent precast concrete box-beam bridges: State of the practice. *PCI J.* **2011**, *56*, 75–91. [CrossRef]
5. Pan, Z.F.; You, F.C. Quantitative design of backup prestressing tendons for long-span prestressed concrete box girder bridges. *J. Bridge Eng.* **2015**, *20*. [CrossRef]
6. Yuan, J.Q.; Graybeal, B. Full-scale testing of shear key details for precast concrete box-beam bridges. *J. Bridge Eng.* **2016**, *21*. [CrossRef]
7. Xue, J.Q.; Briseghella, B.; Lin, J.H.; Huang, F.Y.; Chen, B.C. Design and field tests of a deck-extension bridge with small box girder. *J. Traff. Transp. Eng.* **2018**, *5*, 467–479. [CrossRef]
8. Xu, Z.; Chen, B.C.; Zhuang, Y.Z.; Tabatabai, H.; Huang, F.Y. Rehabilitation and retrofitting of a multispan simply-supported adjacent box girder bridge into a jointless and continuous structure. *J. Perform. Constr. Fac.* **2018**, *32*. [CrossRef]
9. Huang, H.D.; Huang, S.S.; Pilakoutas, K. Modeling for assessment of long-term behavior of prestressed concrete box-girder bridges. *J. Bridge Eng.* **2018**, *23*. [CrossRef]
10. Gupta, T.; Kumar, M. Flexural response of skew-curved concrete box-girder bridges. *Eng. Struct.* **2018**, *163*, 358–372. [CrossRef]
11. Hussein, H.H.; Sargand, S.M.; Steinberg, E.P. Shape optimization of uhpc shear keys for precast, prestressed, adjacent box-girder bridges. *J. Bridge Eng.* **2018**, *23*. [CrossRef]
12. Hussein, H.H.; Sargand, S.M.; Khoury, I. Field investigation of ultra-high performance concrete shear key in an adjacent box-girder bridge. *Struct. Infrastruct. Eng.* **2019**, *15*, 663–678. [CrossRef]
13. Lin, J.H.; Briseghella, B.; Xue, J.Q.; Tabatabai, H.; Huang, F.Y.; Chen, B.C. Temperature monitoring and response of deck-extension side-by-side box girder bridges. *J. Perform. Constr. Fac.* **2020**, *34*, 04019122. [CrossRef]
14. Elbadry, M.M.; Ghali, A. Temperature variations in concrete bridges. *J. Struct. Eng.* **1983**, *109*, 2355–2374. [CrossRef]
15. Dilger, W.H.; Ghali, A.; Chan, M.; Cheung, M.S.; Maes, M.A. Temperature stresses in composite box girder bridges. *J. Struct. Eng.* **1983**, *109*, 1460–1478. [CrossRef]
16. Elbadry, M.; Ghali, A. Thermal stresses and cracking of concrete bridges. *ACI J.* **1986**, *83*, 1001–1009.
17. Mirambell, E.; Aguado, A. Temperature and stress distributions in concrete box girder bridges. *J. Struct. Eng.* **1990**, *116*, 2388–2409. [CrossRef]
18. Massicotte, B.; Picard, A.; Gaumond, Y.; Ouellet, C. Strengthening of long span prestressed segmental box girder bridge. *PCI J.* **1994**, *39*, 52–65. [CrossRef]
19. Saetta, A.; Scotta, R.; Vitaliani, R. Stress analysis of concrete structures subjected to variable thermal loads. *J. Struct. Eng.* **1995**, *121*, 446–457. [CrossRef]
20. Li, D.N.; Maes, M.A.; Dilger, W.H. Thermal design criteria for deep prestressed concrete girders based on data from confederation bridge. *Can. J. Civil. Eng.* **2004**, *31*, 813–825. [CrossRef]
21. Lee, J.H. Investigation of extreme environmental conditions and design thermal gradients during construction for prestressed concrete bridge girders. *J. Bridge Eng.* **2012**, *17*, 547–556. [CrossRef]
22. Rodriguez, L.E.; Barr, P.J.; Halling, M.W. Temperature effects on a box-girder integral-abutment bridge. *J. Perform. Constr. Fac.* **2014**, *28*, 583–591. [CrossRef]
23. Tayşi, N.; Abid, S. Temperature distributions and variations in concrete box-girder bridges: Experimental and finite element parametric studies. *Adv. Struct. Eng.* **2015**, *18*, 469–486. [CrossRef]
24. Abid, S.R.; Tayşi, N.; Özakça, M. Experimental analysis of temperature gradients in concrete box-girders. *Constr. Build. Mater.* **2016**, *106*, 523–532. [CrossRef]
25. Xue, J.Q.; Lin, J.H.; Briseghella, B.; Tabatabai, H.; Chen, B.C. Solar radiation parameters for assessing temperature distributions on bridge cross-sections. *Appl. Sci. Basel* **2018**, *8*, 627. [CrossRef]

26. Liu, Y.J.; Liu, J.; Zhang, N. Review on solar thermal actions of bridge structures. *China Civ. Eng. J.* **2019**, *52*, 59–78.
27. England, G.L.; Tsang, N.C.M.; Bush, D.I. *Integral Bridges: A Fundamental Approach to the Time-Temperature Loading Problem*; Thomas Telford: London, UK, 2000; ISBN 9780727735416.
28. Oesterle, R.G.; Tabatabai, H.; Lawson, T.J.; Refai, T.M.; Volz, J.S.; Scanlon, A. *Jointless Bridges, Summary Report*; Federal Highway Administration: Washington DC, USA, 2005.
29. Zordan, T.; Briseghella, B. Attainment of an integral abutment bridge through the refurbishment of a simply supported structure. *Struct. Eng. Int.* **2007**, *17*, 228–234. [CrossRef]
30. Briseghella, B.; Zordan, T. Integral abutment bridge concept applied to the rehabilitation of a simply supported concrete structure. *Struct. Concr.* **2007**, *8*, 25–33. [CrossRef]
31. Zordan, T.; Briseghella, B.; Lan, C. Parametric and pushover analyses on integral abutment bridge. *Eng. Struct.* **2011**, *33*, 502–515. [CrossRef]
32. Zordan, T.; Briseghella, B.; Lan, C. Analytical formulation for limit length of integral abutment bridges. *Struct. Eng. Int.* **2011**, *21*, 304–310. [CrossRef]
33. Briseghella, B.; Zordan, T. An innovative steel-concrete joint for integral abutment bridges. *J. Traff. Transp. Eng.* **2015**, *2*, 209–222. [CrossRef]
34. Xue, J.Q.; Briseghella, B.; Chen, B.C.; Zhang, P.Q.; Zordan, T. Optimal design of pile foundation in fully integral abutment bridge. In *Developments in International Bridge Engineering*; Caner, A., Gulkan, P., Mahmoud, K., Eds.; Springer International Publishing AG: Cham, Switzerland, 2016; Volume 9, pp. 3–15. ISBN 9783319197852.
35. Huang, F.Y.; Qian, H.M.; Zhuang, Y.Z.; Fu, C. Experimental study on the dynamic response of phc pipe-piles in liquefiable soil. *J. Test. Eval.* **2017**, *45*, 230–241. [CrossRef]
36. Xue, J.Q.; Chen, B.C.; Briseghella, B.; Dong, J.C.; Zhang, P.Q. Design, Construction and monitoring of deck-extension bridge deck in expressway. *J. China Foreign Highw.* **2018**, *38*, 76–82.
37. Xue, J.Q.; Lavorato, D.; Bergami, A.V.; Nuti, C.; Briseghella, B.; Marano, G.C.; Ji, T.; Vanzi, I.; Tarantino, A.M.; Santini, S. Severely damaged reinforced concrete circular columns repaired by turned steel rebar and high-performance concrete jacketing with steel or polymer fibers. *Appl. Sci. Basel* **2018**, *8*, 1671. [CrossRef]
38. Huang, F.Y.; Wu, S.W.; Luo, X.Y.; Chen, B.C.; Lin, Y.W. Pseudo-static low cycle test on the mechanical behavior of PHC pipe piles with consideration of soil-pile interaction. *Eng. Struct.* **2018**, *171*, 992–1006. [CrossRef]
39. Xue, J.Q.; Chen, B.C.; Lin, J.H. Study of temperature expansion and contraction deformation of bridges with their deck slabs extended by hollow slabs. *Bridge Constr.* **2018**, *48*, 37–42.
40. Emerson, M. *Thermal Movements of Concrete Bridges: Field Measurements and Methods of Prediction*; Transport and Road Research Laboratory: Berkshire, UK, 1982.
41. Clark, J.H. Evaluation of Thermal Stresses in a Concrete Box Girder Bridge. Ph.D. Thesis, University of Washington, Washington, DC, USA, 1989.
42. Fang, Z.; Wang, J. Sun light thermal difference effect on long-span pc continuous box girder bridge. *China J. Highw. Transp.* **2007**, *20*, 62–67.
43. Chen, X.Q. Temperature Analysis of Steel-concrete Composite Girder Caused by Solar Radiation. In Proceedings of the Eighteenth National Conference on Structural Engineering, Guangzhou, China, 28 November 2009.
44. Wang, J.; Fang, Z. Temperature variation of concrete box girder bridge. *Front. Archit. Civ. Eng. China* **2009**, *3*, 407–413. [CrossRef]
45. Liu, Y. Research on Temperature Deformation of Extended Slab Concrete Jointless Bridges. Master's Thesis, Fuzhou University, Fuzhou, China, 2016.
46. Zhou, L.R.; Liang, C.F.; Chen, L.; Xia, Y. Numerical simulation method of thermal analysis for bridges without using field measurements. *Procedia Eng.* **2017**, *210*, 240–245. [CrossRef]
47. Lin, J.H.; Briseghella, B.; Xue, J.Q.; Huang, F.Y.; Chen, B.C. Research on influence of material thermal parameters on temperature distribution on cross-section of concrete box girder. *J. Guangxi Univ. (Nat. Sci. Ed.)* **2020**, *45*, 1–8. (in press).
48. Zhang, X.Y. *Practical Handbook of Chemistry*, 2nd ed.; National Defense Industry Press: Beijing, China, 2011; ISBN 7118004243.
49. Zhang, J.Y.; Zhao, L.; Deng, S.; Xu, W.C.; Zhang, Y. A critical review of the models used to estimate solar radiation. *Renew. Sustain. Energy Rev.* **2017**, *70*, 314–329. [CrossRef]

50. Ministry of Transport of the People's Republic of China. *General Specifications for Design of Highway Bridges and Culverts*; JTG D60-2015; China Communications Press: Beijing, China, 2015.
51. National Meteorological Information Center. Available online: http://data.cma.cn (accessed on 28 November 2019).
52. Brooks, C.E.P.; Carruthers, N. Handbook of statistical methods in meteorology. *Geogr. Rev.* **1953**, *44*, 617.
53. Lin, J.H.; Briseghella, B.; Xue, J.Q.; Tabatabai, H.; Chen, B.C.; Huang, F.Y. Research on Effective Temperature of T-Shaped Girder for Jointless Bridges in China. In Proceedings of the 20th IABSE congress, New York, NY, USA, 4–6 September 2019.
54. Duffie, J.A.; Beckman, W.A. *Solar Engineering of Thermal Processes*, 4th ed.; John Wiley & Sons, Inc.: Hoboken, NJ, USA, 2013; ISBN 9781118415412.
55. NASA Prediction of Worldwide Energy Resources. Available online: https://power.larc.nasa.gov (accessed on 28 November 2019).
56. Kehlbeck, F. *Einfluss der Sonnenstrahlung bei Bruckenbauwerken*; Werner: Dusseldorf, Germany, 1975.
57. Ministry of Transport of the People's Republic of China. *Wind-Resistant Design Specification for Highway Bridges*; JTG/T 3360-01-2018; China Communications Press: Beijing, China, 2018.